Modulation of neuronal cell affinity on PEDOT–PSS non-woven silk scaffolds for neural tissue engineering

Adrián Magaz[ab], *Ben F. Spencer*[a], *John G. Hardy*[cd], *Xu Li*[be], *Julie E. Gough*[a], *Jonny J. Blaker*[af]*

[a]Department of Materials and Henry Royce Institute, The University of Manchester, Manchester, M13 9PL, United Kingdom

[b]Institute of Materials Research and Engineering (IMRE), Agency for Science Technology and Research (A*STAR), 138634, Singapore

[c]Department of Chemistry, Lancaster University, Lancaster, LA1 4YB, United Kingdom

[d]Materials Science Institute, Lancaster University, Lancaster, LA1 4YB, United Kingdom

[e]Department of Chemistry, National University of Singapore, 117543, Singapore

[f]Department of Biomaterials, Institute of Clinical Dentistry, University of Oslo, Oslo, 0317, Norway

*Corresponding author, email: jonny.blaker@manchester.ac.uk

KEYWORDS: PEDOT–PSS; silk fibroin; electrospinning; neuronal scaffold

ABSTRACT

Peripheral nerve injury is a common consequence of trauma with low regenerative potential. Electroconductive scaffolds can provide appropriate cell growth microenvironments and synergistic cell guidance cues for nerve tissue engineering. In the present study, electrically conductive scaffolds were prepared by conjugating poly(3,4-ethylenedioxythiophene)-polystyrene sulfonate (PEDOT–PSS) or dimethyl sulfoxide (DMSO)-treated PEDOT–PSS on electrospun silk scaffolds. Conductance could be tuned by the coating concentration and was further boosted by DMSO treatment. Analogue NG108-15 neuronal cells were cultured on the scaffolds to evaluate neuronal cell growth, proliferation and differentiation. Cellular viability

was maintained on all scaffold groups, while showing comparatively better metabolic activity and proliferation than unmodified silk. DMSO-treated PEDOT–PSS functionalized scaffolds partially outperformed their PEDOT–PSS counterparts. Differentiation assessments suggested that these PEDOT–PSS assembled silk scaffolds could support neurite sprouting, indicating that they show promise to be used as a future platform to restore electrochemical coupling at the site of injury and preserve normal nerve function.

1. INTRODUCTION

Electroconductive scaffolds have shown great promise in engineering electrically sensitive tissues such as muscle (e.g. cardiac, skeletal, smooth) and nerve,[1] which are highly dependent on electrochemical signaling between or within cells.[2] Materials that are intended to interact with tissues should be engineered to stimulate the wound healing response. In particular, neural tissue exhibits low regenerative potential. Since electrical integrity is essential for the repair and regeneration process of the nervous system, different avenues to improve conduction of biomaterials and enhance tissue function have been explored over the years, as recently reviewed.[1,3]

Conjugated polymers such as polypyrrole (PPy), polyaniline (PANI) and poly(3,4-ethylene-dioxythiophene) (PEDOT) are attractive candidates in tissue engineering due to their versatility in many biomedical applications and highly electrically conductive nature.[4,5] PEDOT is the most studied polythiophene derivative due to its higher electrical conductivity and chemical stability.[6] Unlike other conductive polymers, PEDOT doped with polystyrene sulfonate (PEDOT–PSS) is easily dispersed in aqueous solution, it is amenable to solution processing and retains a significant amount of its conductive properties in physiological conditions.[7,8] Accordingly, the use of PEDOT–PSS is a promising candidate for developing conductive scaffolds[9–11] with the ability to support cell adhesion, and facilitate cell growth and

differentiation. PEDOT–PSS transduces charge by both ion and electron/hole exchange.[12] Its conductance can be further optimized by treatment with polar solvents such as dimethyl sulfoxide (DMSO), a process by which the anionic PSS shells are partially washed away leading to a shift in the structure of disentangled PEDOT–PSS with more efficient orbital overlap and interchain packing for charge transport.[13] The use of pure conjugated polymers tends to be limited, though, due to their poor processability, non-degradability, brittle behavior and tendency to crack attributed to the tight coil-like conformation in the polymer backbone.[14] Therefore, they are usually incorporated via blending or coating with another polymer.

An important cue in tissue engineering is the recapitulation of the fibrillary topography of native tissues, where many of the major components of the extracellular matrix (ECM) exist as fibers that mediate cellular responses such as attachment, migration, growth, proliferation and differentiation.[15,16] Myriad micro-/nano-fabrication technologies for engineering fibrous scaffolds for tissue engineering applications have been developed over the years.[17] Electrospinning remains the most common technique to manufacture micro-/nano-fibrous structures at the multiscale with high surface area to volume ratio and defined spatial density both in 2D and 3D.[18]

Silk fibroin is readily available from silkworm cocoons (e.g. *Bombyx mori*), and has been demonstrated to support the growth of a wide range of cell types *in vitro* and tissue ingrowth *in vivo*.[19–21] The relatively ease of its processing, along with the versatility of the physico-chemical and mechanical properties of silk, has made it one of the most commonly used naturally-occurring proteins for biomedical applications.[21,22] Previous studies have reported the testing and manufacture of electroconductive/active scaffolds based on silks and the incorporation of carbon-based nanomaterials or metallic nanoparticles, as reviewed in [23]. Functionalization with conjugated polymers could be a more direct approach to achieve

excellent electrical conductivity for enhanced cellular signaling response. The combination of PEDOT and silk has been primarily explored in the area of microelectronics,[24–30] with some reports studying their biological response in biosensor devices.[31,32] Even less attention has been paid to hybrid scaffolds made of PEDOT and silk for regenerative medicine applications.[33]

In this study, fibrous scaffolds based on silk fibroin were fabricated by electrospinning and rendered conductive by functionalization with PEDOT–PSS or DMSO-treated PEDOT–PSS. NG108-15 neuronal cells were seeded to assess the biological response of these substrates. The contribution of PEDOT could enhance the neuronal cell response in terms of adhesion, proliferation and neurite outgrowth.

2. EXPERIMENTAL SECTION

2.1 Preparation of regenerated silk fibroin

Extraction and purification of silk fibroin (SF) from *Bombyx mori* was carried out following a previously described protocol[34] based on a degumming process to remove sericin and lithium bromide dissolution of the degummed fibers, followed by dialysis against water for 3 days. The resulting regenerated SF solution was cast onto polystyrene dishes (Sigma-Aldrich, UK) and dried in a forced air-circulation oven (Memmert Universal, Germany). SF films were peeled off and kept as stock material for further use.

2.2 Fabrication of electrospun silk scaffolds

Regenerated SF films were dissolved in 1,1,1,3,3,3-hexafluoro-2-propanol (HFIP) (Sigma-Aldrich, UK) at 10% w v^{-1} and subsequently electrospun into fibers. Scaffolds were spun using a single needle, targeted towards a static collector using a custom-built electrospinning set-up with the following parameters: continuous flow rate, 0.8 mL h^{-1}; tip-to-collector distance, 10 cm; applied voltage, 15 kV; relative humidity, 25%; needle gauge, 19 G. As-spun scaffolds were annealed by immersion in a bath of 80% v v^{-1} ethanol to induce β-sheet conformational

transition, dried overnight between filter paper to prevent folding, and stored in a desiccator for further use.

2.3 Surface functionalization of silk scaffolds with PEDOT–PSS and DMSO-treated PEDOT–PSS

Electrospun SF scaffolds were functionalized with poly(3,4-ethylenedioxythiophene) polystyrene sulfonate (PEDOT–PSS) or dimethyl sulfoxide (DMSO)-treated PEDOT–PSS (**Scheme 1A-B**), wherein the PEDOT and PSS interact primarily through electrostatic interactions yielding highly durable conductance on degummed silk-based materials.[28]

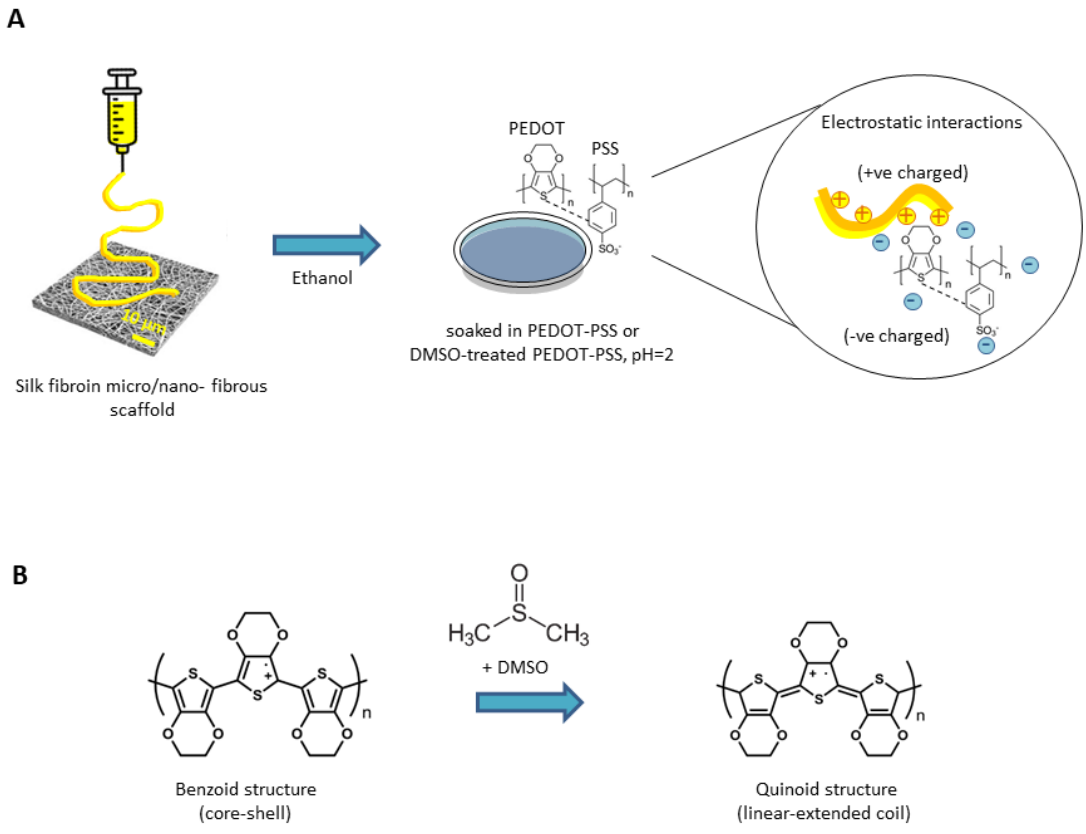

Scheme 1 (**A**) Schematic of electrospun silk fibroin scaffolds followed by conjugation with PEDOT–PSS or DMSO-treated PEDOT–PSS. (**B**) Schematic of the conformational change of the PEDOT–PSS structure after treatment with DMSO, from core-shell (i.e. benzoid) towards linear-extended coil (i.e. quinoid).

Silk fibroin has an isoelectric point at pH 4-5,[35,36] meaning the polypeptide fibers will become positively charged under sufficiently acidic conditions, and the isolelectric point of PSS is ca. 1.2-1.5 dependent on the salt concentration (i.e. deprotonated above pH 1.5),[37]consequently the materials were processed under acidic conditions (pH = 2) to ensure a high level of electrostatic attraction between PEDOT–PSS and silk during processing. PEDOT–PSS aqueous dispersions were prepared from a commercial solution (pH = 2, supplied at a 1.3% wt. dispersion in water) (Sigma-Aldrich, UK) at different concentrations (0.5, 1, 3, 9, 13 mg mL^{-1}). SF scaffolds (13 mm diameter, ~100 μm thickness, ~80% porosity and ~15 μm pore dimension) were submerged (1 mL per scaffold) in the prepared PEDOT–PSS solutions and sonicated in a room temperature controlled water bath for 1 h (37 Hz; Elmasonic P60H, Germany). Scaffolds were then rinsed (× 2 times) in deionized (DI) water to remove excess PEDOT–PSS and air-dried for 2 h at room temperature. This dyeing-drying process was repeated twice. Based on the PEDOT–PSS solution concentration (ranging from 0.5 to 13 mg mL^{-1}), the functionalized scaffolds were named SF-0.5P (0.5), SF-1P (1), SF-3P (3), SF-9P (9) and SF-13P (13). Separately, DMSO-treated PEDOT–PSS solutions were prepared by mixing 95% v v^{-1} of PEDOT–PSS with 5% v v^{-1} DMSO (Sigma-Aldrich, UK), vortexed and allowed to settle overnight. A similar process as described above was carried out to give SF-0.5PD, SF-1PD, SF-3PD, SF-9PD and SF-13PD scaffolds. The PEDOT–PSS and DMSO-treated PEDOT–PSS uptake mass on the produced scaffolds (13 mm diameter, n=3 per scaffold type) was estimated based on weight differences before and after functionalization, while the concentration was calculated by taking into account the dilution factor of the solution and the porosity of the scaffolds.

2.4 Zeta potential and particle size measurements

The zeta potential and particle size of PEDOT–PSS and DMSO-treated PEDOT–PSS were determined using a Zeta Sizer Nano dynamic light scattering (DLS) instrument (Malvern Panalytical, SG). Aliquots (n=3 per type) of freshly prepared dispersions (0.2 mg mL^{-1}) were pipetted into disposable folded capillary cells (DTS1070) (Malvern Panalytical, SG) and used for measurements in a volume of 750 µL. A refractive index of 1.334 was used for PEDOT–PSS, according to the manufacturer. Three measurements, with 10-100 runs each, were taken per sample at 25° C with an equilibration time of 30 s. Zetasizer software (Malvern Panalytical, SG) was used for data analysis.

2.5 Characterization of the scaffolds

2.5.1 Morphology and surface topography

Field emission scanning electron microscope (FESEM) images from different batches of samples were taken using a JEOL JSM6700F at an accelerating voltage of 5 kV and ~ 8 mm working distance. Fiber diameter size distribution was analyzed with Fiji 1.28 (NIH, USA); a minimum of 100 individual fibers per sample were analyzed.

2.5.2 Hard X-ray photoelectron spectroscopy

The surface and bulk-like compositions of the functionalized scaffolds were quantitatively analyzed with a high-throughput lab-based hard X-ray photoelectron spectroscope (HAXPES, Scienta Omicron) equipped with a Ga Kα X-ray source (9.25 keV; Excillum). For measurements, scaffolds were mounted on Omicron flag-style sample plates using double-sided adhesive copper tape. The survey spectra were measured using an EW4000 electron energy analyzer with 500 eV pass energy and ~2 eV energy resolution. Core level spectra of elements of interest were measured with 200 eV pass energy and ~0.8 eV energy resolution [38]. Atomic concentrations were calculated based on sensitivity factors for the core levels, as listed in [39]. The sampling depth for HAXPES was calculated using the TPP-2M formula to be ~54

nm, and surface sensitive XPS using a standard Al Kα X-ray source (1.486 keV) was also performed with a sampling depth of ~11 nm; the operating pressure was 6×10^{-10} mbar. Quantitative analysis of spectra was carried out with CasaXPS (v. 2.3.23) processing software in the range of 160–175 eV (S 2p, XPS, ~11 nm) and 2460–2485 eV (S 1s, HAXPES, ~54 nm) (**Figure S1**). The PSS and PEDOT peaks were fitted using Voigt-approximation Gaussian-Lorenztian peaks and the PSS to PEDOT ratios were subsequently calculated. PSS and PEDOT are easily identified in the spectra since PSS is chemically shifted by 4 eV to higher binding energy than PEDOT for the S 2p core level measured with XPS, and 5 eV for the S 1s core level measured with HAXPES.[40]

2.5.3 Protein adsorption

The ability of the scaffolds (n=3 per type) to adsorb protein was evaluated with bovine serum albumin (BSA) (Sigma-Aldrich, UK), quantified with a Pierce™ bicinchoninic acid (BCA) protein assay kit (Thermo Fisher Scientific, UK) based on the amount of remaining BSA in solution after adsorption. Samples were incubated at 37°C overnight in 1 mL of 500 μg mL^{-1} BSA in DI water. Absorbance was measured at 562 nm using a microplate reader (Infinite M200) (Tecan Life Sciences, SG). The amount of protein was calculated using a standard curve obtained from BSA within the range of measured concentrations. All samples were conducted in triplicate. Scaffolds incubated in DI water served as blanks, and DI water was used as negative control.

2.5.4 Surface roughness

Surface morphology was assessed using a Countour GT-K1 3D optical profilometer (Veeco, USA). Briefly, scaffolds (n=2 per type) were placed on glass coverslips and fixed with ethanol to ensure a near flat surface. They were then pre-conditioned in supplemented culture media overnight and dehydrated in a series of ethanol solutions prior to imaging. Samples were

imaged in vertical scanning interferometry mode. A total of 10 micrographs (66 μm × 87 μm) were taken per sample at different fields of view, with an average of five measurements per image. Analysis of the surface roughness (arithmetical mean surface height (Sa) and root mean square surface height (Sq)) based on 3D profile ordinates was performed with the Vision64 Map™ (Bruker, USA) software.

2.5.5 Electroconductive properties

An automated 4-point probe electrical conductivity and resistivity station (A4P-200 MicroXACT) connected to a combined DC current source and digital voltmeter (Jandel RM3000) was used for the experiments.[10,41,42] Conductivity was estimated at room temperature (~20°C) in four different locations on each scaffold (n=4 per type), in the dry state and in the hydrated state after overnight incubation in phosphate buffered saline (PBS). Excess water was removed using blotting paper prior to taking the readings.

2.5.6 Chemical structure

Chemical bond analysis of the functionalized scaffolds was conducted using Fourier transform infrared (FTIR) spectroscopy. PEDOT–PSS and DMSO-treated PEDOT–PSS solutions were cast on a petri dish, let air-dry overnight and peeled off as films for comparison. FTIR spectra were taken with a PerkinElmer 2000 spectrometer equipped with a zinc selenide (ZnSe) crystal in attenuated total reflectance (ATR) mode, in the range 4000-600 cm^{-1} and resolution 4 cm^{-1}, with 32 scans taken per measurement.

2.6 *In vitro* study

2.6.1 NG108-15 culture

Analogue NG108-15 neuronal cells were grown in NG108-15 growth medium as previously described [43] and used between passage P17-30.

For cell culture experiments, functionalized scaffolds (13 mm diameter) were positioned onto CellCrown™ polycarbonate inserts (Scaffdex Oy, Finland) for 24-well plates. Scaffolds were maintained in molecular biology grade water (AccuGENE™) (Lonza, UK) for 24 h, air-dried and sterilized under UV light (30 min on each side, top and bottom) in a class II biosafety cabinet. Glass coverslips (CV) (12 mm diameter, 0.13-0.16 mm thickness) (VWR, UK) served as positive controls. Scaffolds were preconditioned in supplemented media and seeded at a density of 20,000 cells per well with minimum media to ensure maximum cell attachment (~2 h) before being topped up to 1 mL. The culture was maintained for 7 days, with half of the medium changed every other day.

2.6.2 Cell viability, metabolic activity and proliferation

Cellular viability was measured at specific time intervals on cells on the scaffolds (n=2 per type) with a LIVE/DEAD® viability/cytotoxicity fluorescence kit (Thermo Fisher Scientific, UK) following the manufacturer's instructions. Samples were 3D imaged using a TCS SP8 confocal laser scanning microscope (Leica Microsystems, UK). Data is expressed as the percentage of live cells versus non-viable/dead cells, analyzed from several fields of view.

The metabolic activity of cells on the scaffolds (n=3 per type) was monitored with the alamarBlue™ reduction assay based on resazurin sodium salt (Sigma-Aldrich, UK). Metabolic activity is expressed relative to dsDNA concentration – quantified using a Quant-i™ PicoGreen® dsDNA assay kit (Thermo Fisher Scientific, UK) following the manufacturer's instructions. Cellular proliferation is expressed in terms of cell number, estimated based on a single cell's DNA content.[44]

2.6.3 Differentiation and neurite outgrowth

To induce terminal differentiation, cells were grown in serum-free culture media. The culture was maintained for 5 days, with half of the media removed and replaced with fresh media every

other day. After 5 days of culture, cell-laden scaffolds (n=2 per type) were harvested, fixed, permeabilized and blocked against non-specific binding. Differentiated cells on the scaffolds were stained with polyclonal rabbit anti-mouse/rat ß-tubulin III (Abcam, UK) conjugated to Alexa Fluor® 488 (Abcam, UK) (1:1000 v v^{-1} dilution). Cell nuclei were counterstained with 4,6-diamidino-2-phenylindole dihydrochloride (DAPI) (Sigma-Aldrich, UK). Samples were mounted and 3D imaged with a TCS SP8 confocal laser scanning microscope (Leica Microsystems, UK).

For analysis of cell differentiation, neurite length was determined on a cell-by-cell basis on each scaffold type from immunofluorescent micrographs using Fiji software. Only cell processes longer than 30 µm were considered for analysis, with a minimum of 10 neurites analyzed per sample.

2.7 Data analysis

Statistical analysis was performed with GraphPad Prism 8 (San Diego, USA), and datasets checked for normality. Normally distributed data is presented as standard deviation (SD, error bars) of the mean values. For parametric data and multiple comparisons, significance was assessed by one-way ANOVA (one independent variable) or two-way ANOVA (two independent variables) using Tukey's post hoc analysis test. For comparing parametric data between two groups, two-tailed unpaired Student's t-test was used. Not normally distributed data was assessed by Kruskal-Wallis with Dunn's post hoc analysis test. A value of $p<0.05$ was considered statistically significant.

3. RESULTS AND DISCUSSION

This work aims to develop an electroconductive silk-based scaffold which can enhance maturation and physiological properties of engineered nerve tissues. For this purpose, the (bio)functionality of silk fibroin was harnessed together with the inherent highly

electroconductive property of PEDOT–PSS, which was further boosted by DMSO treatment. Treatment of PEDOT–PSS with DMSO resulted in an increase in particle size (**Figure S2A**) based on DLS analysis,[11] with no significant change in surface charge (**Figure S2B**). It has been reported that the geometry of PEDOT–PSS changes from coil-structure towards a more linear-extended morphology after DMSO treatment.[45] While the DLS technique assumes a spherical model acceptable for PEDOT–PSS, it can still provide a reasonable estimate of the order of magnitude in the case of DMSO-treated PEDOT–PSS.

Native neural tissue is comprised of several structural fibrillary proteins ranging from several nanometers to micrometers in diameter.[46] Consequently, the fabrication of biomimetic fibrous structures plays a key role in the properties of tissue engineered scaffolds. Visual appearance and fiber morphology of the scaffolds are shown in **Figure 1A-B**. Compared to neat silk, which is whitish in appearance, scaffolds became increasingly darker blue upon functionalization, qualitatively indicating that the coverage amount on the scaffolds increased gradually with increasing amounts of PEDOT–PSS or DMSO-treated PEDOT–PSS. Likewise, increased mass uptake of PEDOT–PSS or DMSO-treated PEDOT–PSS on the scaffolds was observed at increasing coating concentration (**Table S1**). This was further confirmed by FESEM analysis. FESEM micrographs revealed PEDOT particles attached on the surface of the fibers to different extents based on the coating concentration, with some inter-fiber pores partially occluded at high coating concentrations. The random fiber distribution and inter-fiber porosity of the scaffold may have favored this. In contrast, a highly aligned fibrous scaffold with increased fiber packing density and diminished porosity[47] is more likely to reduce the inter-fibre pore dimension,[48] which may in turn affect the penetrating efficiency of PEDOT–PSS. Analysis of the fiber diameter size distribution (**Figure 1C**) demonstrated some differences

after functionalization compared to neat silk. The average fiber diameter size remained ~0.5 μm for all samples.

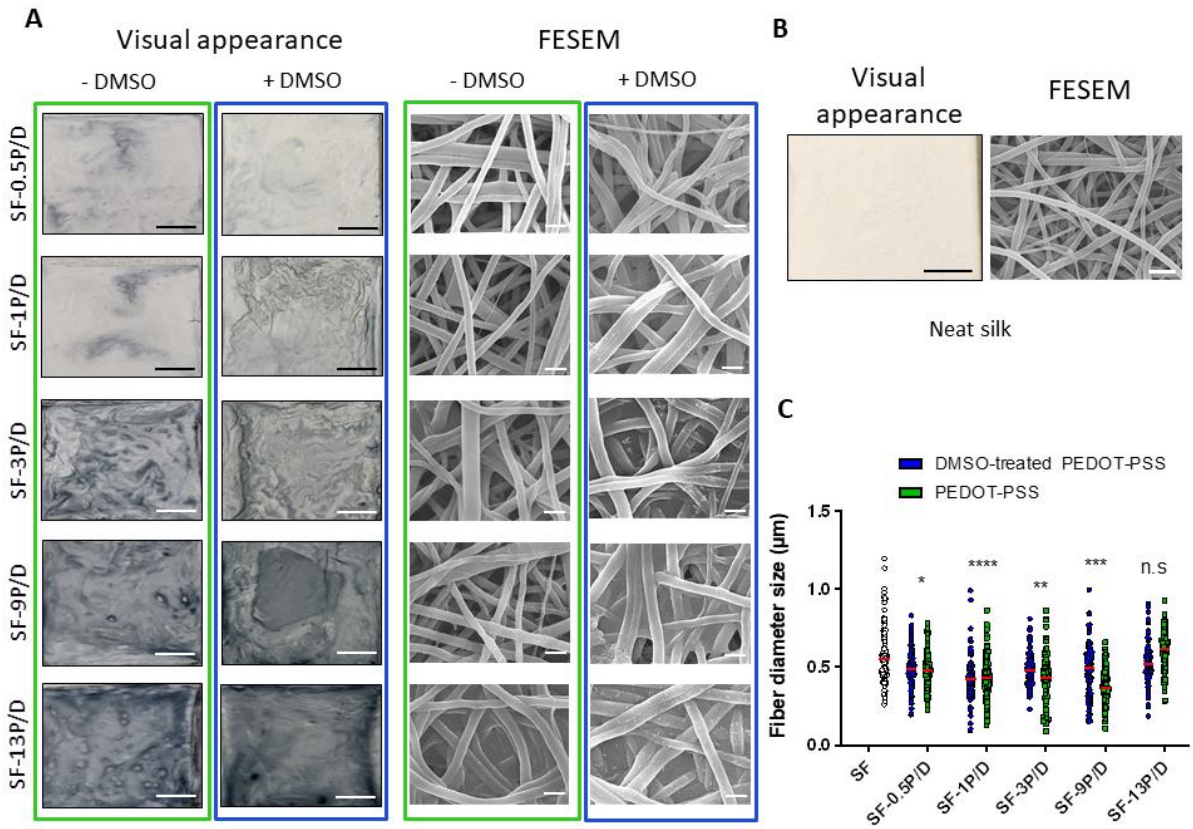

Figure 1 Effect of PEDOT–PSS and DMSO-treated PEDOT–PSS conjugation on scaffold microstructures. (**A**) Representative visual appearance and FESEM micrographs of the different scaffolds after functionalization at increasing concentration; scale bars at 3 mm and 900 nm, respectively. (**B**) Representative visual appearance and FESEM micrograph of neat silk; scale bars at 3 mm and 2 μm, respectively. (**C**) Fiber diameter size distributions of the various scaffolds. Differences between the experimental groups were analyzed by Kruskal-

Wallis with Dunn's test, compared to unmodified silk. n.s non-significant, *p<0.05, **p<0.01, ***p<0.001, ****p<0.0001.

The long-term stability of the PEDOT–PSS and silk fibroin interface had been previously demonstrated.[28] Under acidic conditions for PEDOT–PSS and DMSO-treated PEDOT–PSS, a minimal decrease in conductivity was observed after several consecutive dry-cleaning cycles, confirming the importance of favorable electrostatic interactions.[28] Under less acidic conditions, functionalization was less successful.[28]

The relative percentage of sulfur (S) in the produced scaffolds, representing PEDOT and PSS, is shown in **Figure S3A** in a concentrated-dependent manner at increasing coating concentration after functionalization. As expected, higher relative S percentage is observed at the surface (~11 nm) rather than at the bulk-like (~54 nm) of the scaffolds. A decrease in the relative ratio of PSS to PEDOT both at the surface and bulk-like of the scaffolds was also observed (**Figure S3B)** after DMSO-treated PEDOT–PSS functionalization. This is likely to be due to the accepted conclusion that DMSO treatment of PEDOT–PSS removes excess of anionic PSS chains, in line with previous studies on films.[49,50] We show this is also true for the fibrous functionalized scaffolds investigated here.

The ability of the scaffolds to adsorb and retain bovine serum albumin, as a model protein, was investigated to assess the functionalized scaffolds. Cell-material interactions can be affected by surface chemistry and the physical features of the substrate onto which cells adhere.[51] For instance, differences in surface roughness have been shown to modulate cell adhesion, proliferation and differentiation of a variety of different cell types through surface adsorption of proteins.[52,53] The amount of BSA retained on the scaffolds is shown in **Figure 2A**. Greater amounts of protein were adsorbed on the functionalized scaffolds, further boosted at increased PEDOT content. While surface roughness increased after PEDOT functionalization compared

to unmodified silk, no significant differences were observed among the various functionalized scaffolds (**Figure 2B**, **Figure S4**). Therefore, the greater protein adsorption observed here at increased PEDOT content could have primarily been influenced by alterations in local electrostatic interactions[54,55] and by electrical charges[56] attributed to the endogenous electrical regimes of the conjugated polymer. Indeed, BSA is negatively charged under physiological conditions since its isoelectric point is around 4.7.[57] If anionic PSS is partially washed away during PEDOT–PSS treatment with DMSO,[13] the scaffold's surface will be less negatively charged which will clearly have an effect on the adsorption of proteins and other biomolecules on their surfaces (**Figure 2A**).

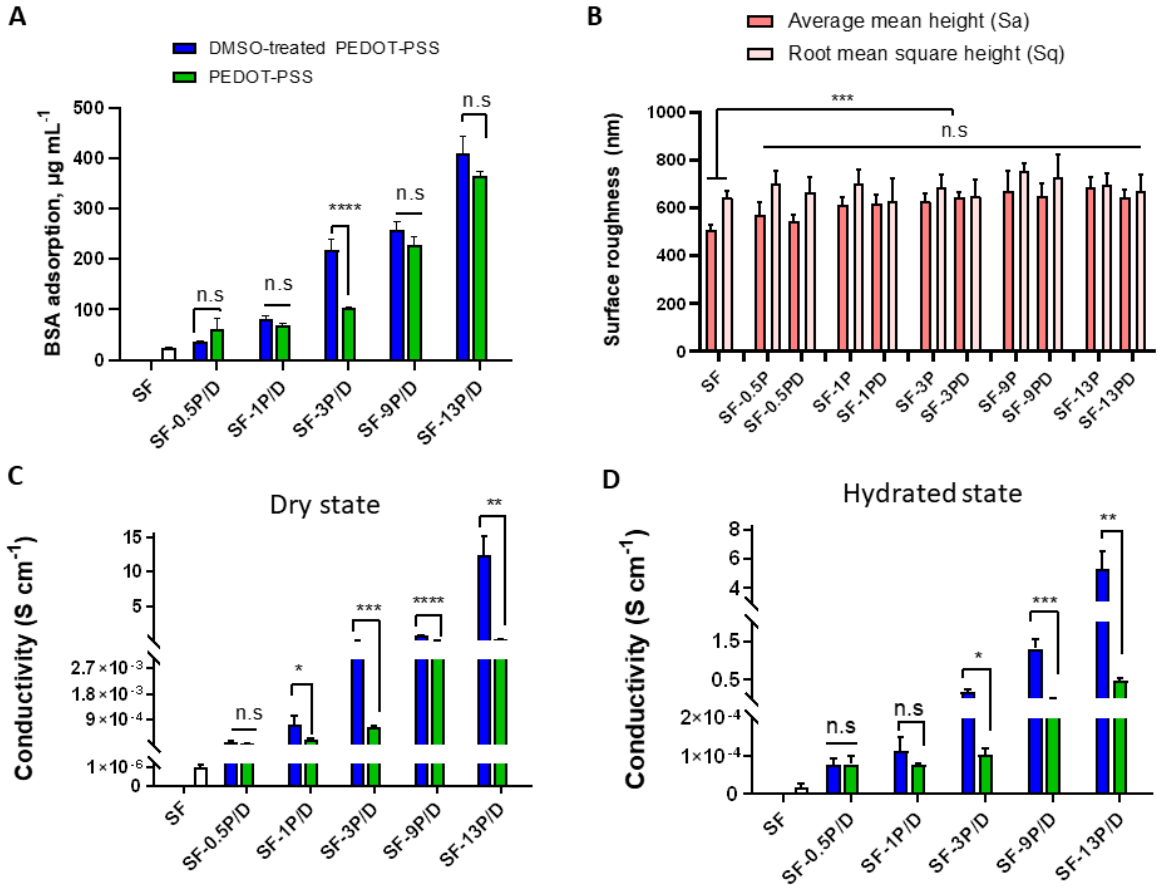

Figure 2 Effect of PEDOT–PSS and DMSO-treated PEDOT–PSS on protein adsorption, surface roughness and conductivity. (**A**) Quantification of BSA adsorption on the various

scaffolds (n=3 per type). (**B**) Quantitative analysis of surface roughness of the scaffold (n=2 per type). (**C-D**) Electroconductivity of the scaffolds (n=4 per type) in the dry and hydrated states. Differences between the experimental groups were analyzed by two-way ANOVA with Tukey's post hoc test. n.s. non-significant, *p<0.05, **p<0.01, ***p<0.001, ****p<0.0001.

Electrical conductivity of the scaffolds was estimated via 4-point probe testing (**Figure 2C-D**, **Table S2**). Neat silk can be considered as a low proton/ion conductor;[58] here the scaffolds became highly conductive with the incorporation of PEDOT–PSS. Conductance could be tuned in the dry state in the range $\times 10^{-5}$ to 10^{-1} S cm^{-1} by varying the coating concentration used for functionalization (**Figure 2C**). Treatment of PEDOT–PSS with DMSO resulted in a substantial enhancement of the conductivity of the scaffolds compared with their PEDOT–PSS counterparts. Indeed, several methods have been investigated to boost PEDOT–PSS conductivity.[45,59,60] Solvent treatment with DMSO is widely used amongst other polar solvents such as methanol, dimethylformamide, tetrahydrofuran or ethylene glycol.[59] It has been postulated that the PSS chains are partially washed away during solvent treatment,[60] with the structure of PEDOT changing from benzoid (i.e. coil conformation) to quinoid (i.e. linear-extended coil conformation).[45] Disentangled PEDOT–PSS leads to alterations in orbital overlap and more efficient interchain packing, inducing the formation of π-stack lamellas and creating a better pathway for charge transport, thereby boosting conductivity.[13] Conductivity of the scaffolds was also characterized in a wet state after hydration overnight (**Figure 2D**). No predominant changes were reported compared to their dry-state counterparts (**Table S2**). This suggests that the electron/ion charge provided by PEDOT tends to dominate over the ionic charges mainly attributed to the aqueous environment. In this regard, some authors have observed an increase in conductivity when scaffolds have been saturated in culture media or other aqueous environments,[41] in contrast to others who have observed a substantial

decrease.[1,61] This demonstrates the difficulty to decouple the electronic contribution of conductive moieties with respect to the ionic contribution of buffered electrolytes. Favorable electrostatic interactions between PEDOT–PSS and silk fibroin had been previously demonstrated to maintain stable conductive properties over time,[28] but it is expected that with sufficiently long periods of incubation, some particles would end up being detached. This strategy is not one without limitations, and longer stability may be achieved by forming interpenetrating networks by means of *in situ* polymerization of the monomers on the scaffold.[6]

FTIR-ATR was performed (**Figure 3**) to explore the change of the surface chemical groups on the scaffolds. The typical fingerprint regions of silk were observed in the spectrum of the neat sample, with peaks corresponding to the amide I (1700-1600 cm^{-1}), II (1600-1500 cm^{-1}) and III (1300-1200 cm^{-1}) bands.[62] The bands corresponding to the amide I and II regions slightly shifted after coating with PEDOT–PSS or DMSO-treated PEDOT–PSS. These changes suggest that PEDOT–PSS interacts (e.g. electrostatic interactions and hydrogen bond interactions) with the silk (notable as sulfate anions [like those displayed on PSS] are kosmotropic anions that encourage "salting out" of protein chains from solution). The characteristic vibration frequencies corresponding to β-sheets were present in all functionalized scaffolds, indicating the retention of the secondary structure of silk after the chemical modification process with PEDOT–PSS. The intensity of the silk peaks gradually decreased with increasing concentration of PEDOT–PSS on the scaffolds. The peak corresponding to the amide III region (1300-1200 cm^{-1}) was not fully observed in the spectra at high coating concentrations. Some distinguishing peaks previously reported typical of PEDOT–PSS[24] could be observed in the spectra: peaks at around 1005 (SO_3 symmetric stretching vibrations),[63] 976 and 835 cm^{-1} (C–S–C deformation vibration). The double peaks observed at around 2920 and 2850 cm^{-1} correspond to C–H

stretching vibrations.[64] FTIR-ATR spectra of PEDOT–PSS and DMSO-treated PEDOT–PSS are shown in **Figure S5**.

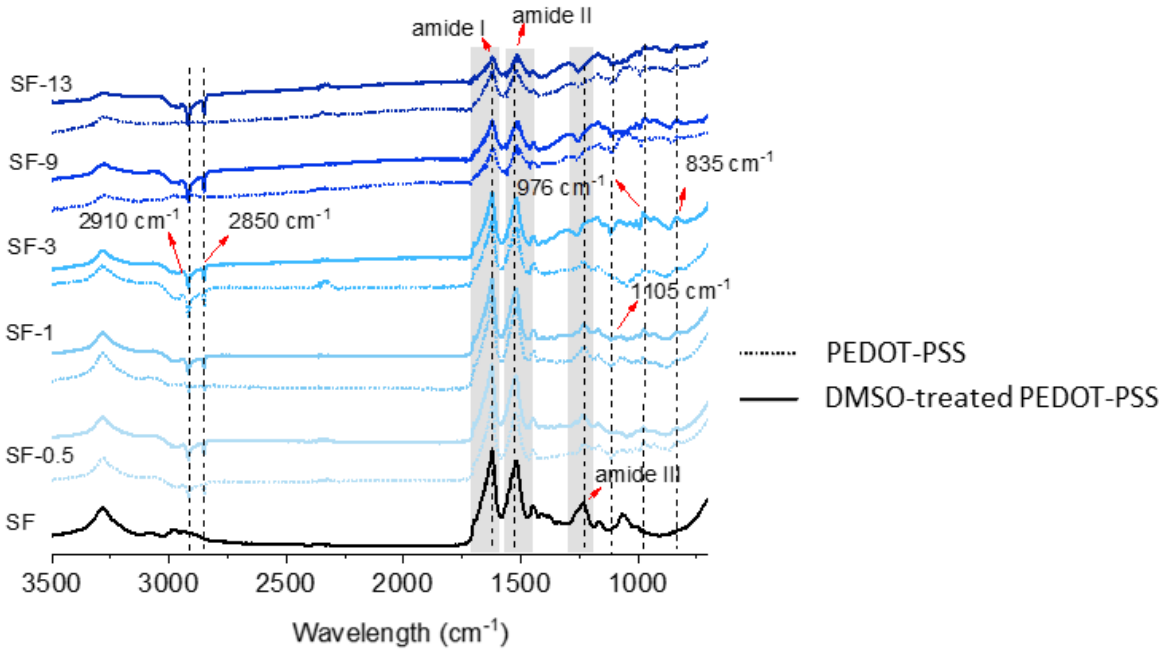

Figure 3 Representative FTIR spectrum showing the typical fingerprint of silk fibroin, along with some characteristic peaks attributed to PEDOT–PSS.

Here we demonstrate that systematic variations in the formulation of PEDOT–PSS result in silk-based scaffolds with highly tunable electroconductivity. These scaffolds may support the electrical pathways of nerve tissue by aiding in the propagation of electrical signals among neurons. Nerve tissues are electrically sensitive, and neurons rely on electrical stimuli for maintaining tissue homeostasis and function. Electroconductive scaffolds hold great potential for nerve tissue engineering since they can promote the propagation of electrical impulses. The ability of the functionalized scaffolds (PEDOT–PSS and DMSO-treated PEDOT–PSS; coating concentrations at 0.5 mg/mL – low, 3 mg/mL – medium, and 13 mg/mL – high) to support neuronal cell growth and differentiation was evaluated with NG108-15 neuronal-like cells.

Presence of low to high contents of PEDOT–PSS or DMSO-treated PEDOT–PSS on the scaffolds did not have major cytotoxic effects over the cell culture period compared to glass coverslip or unmodified silk (**Figure 4, Figure S6**). Representative confocal micrographs of viable and non-viable cells laden on the various scaffolds are shown in **Figure 4A** and **Figure S6A**, indicating increased cell coverage in a time-dependent manner. After 7 days of culture, cells on the scaffolds remained highly viable for every group tested (**Figure 4B, Figure S6B**).

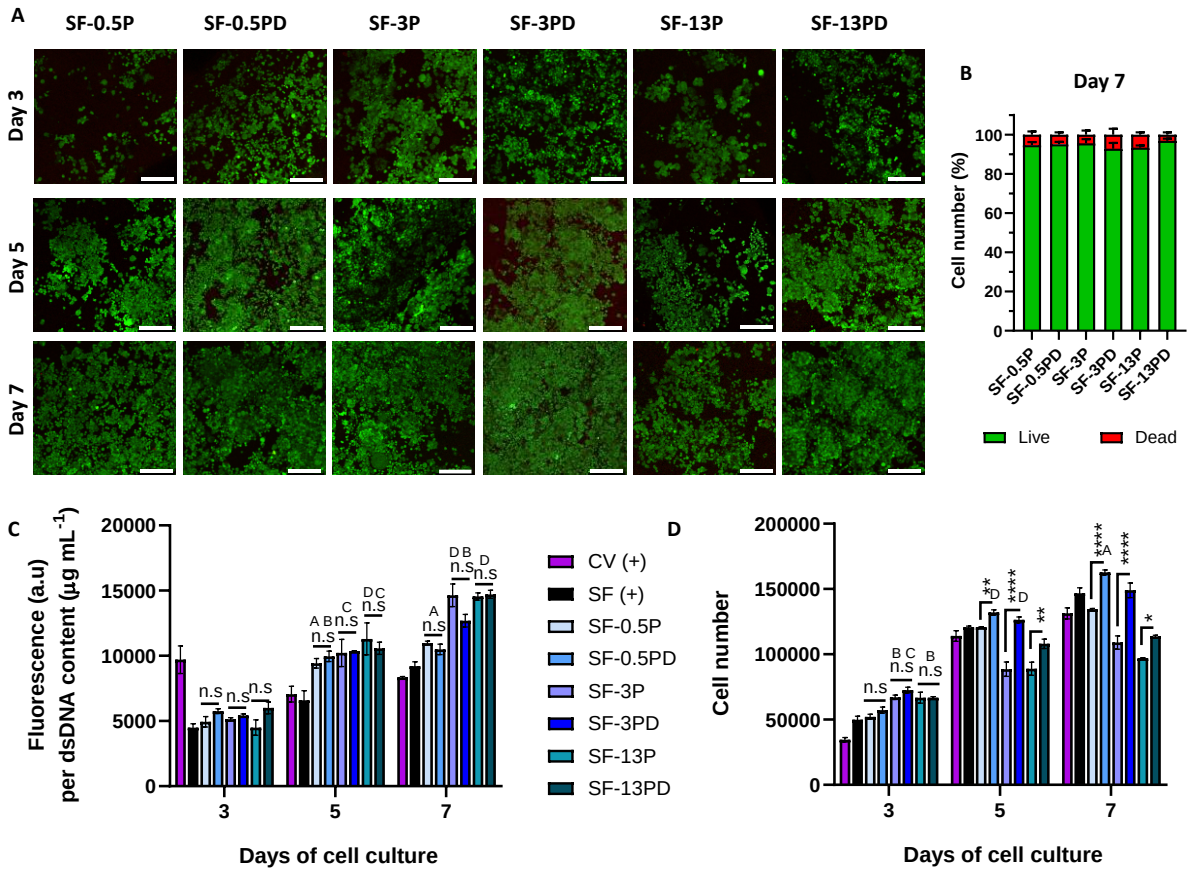

Figure 4 (A-D) Cellular viability, metabolic activity and proliferation of NG108-15 cells on PEDOT–PSS and DMSO-treated PEDOT–PSS functionalized scaffolds (low, medium, and high coating concentration) over a 7-day period. (**A**) Representative confocal micrographs showing cellular viability: viable cells are labeled with calcein AM (green) and dead cells are labeled with ethidium homodimer-1 (red); scale bar at 250 µm. (**B**) Semi-quantitative analysis

of the percentage of viable and non-viable cells after 7 days of culture (n=2 scaffolds per type). (**C**) Metabolic activity relative to dsDNA content (n=3 scaffolds per type). (**D**) Cellular proliferation (n=3 scaffolds per type). Differences between the experimental groups were analyzed by two-way ANOVA with Tukey's post hoc test. n.s. non-significant, *$p<0.05$, **$p<0.01$, ****$p<0.0001$; (with respect to silk fibroin: $^{A}p<0.05$; $^{B}p<0.01$; $^{C}p<0.001$; $^{D}p<0.0001$).

The metabolic activity of NG108-15 cells seeded on the scaffolds **(Figure S7A)** is shown as a function of the dsDNA concentration in **Figure 4C**, giving an indication of the metabolic activity of the culture relative to the number of cells present on it. Cells remained metabolically active on all scaffold groups, with their profile increasing steadily over time. Cells were metabolically more active on the functionalized scaffolds compared to unmodified silk. No significant differences were observed between the DMSO-treated PEDOT–PSS and PEDOT–PSS counterparts, but the tendency observed was for cells to be metabolically more active on scaffolds functionalized at higher coating concentration. Cellular proliferation, on the other hand, exhibited a different trend (**Figure 4D, Figure S7B**), demonstrating greater cellular response on the functionalized scaffolds at the DMSO-treated PEDOT–PSS interface as opposed to PEDOT–PSS. Scaffolds functionalized with the high coating concentration exhibited lower proliferation after 7 days of culture. This indicates that while low to medium contents of PEDOT could be beneficial to NG108-15 cells, too much coating may hinder their proliferation.

The outgrowth of neurites and axonal elongation is under complex control and is essential for building functional neural circuits during regeneration, vital for the function of neuronal cells. Differentiation of NG108-15 cells on the scaffolds was morphologically assessed after 5 days of culture with a marker for ß-tubulin III (**Figure 5A,** zoomed-in confocal micrographs in

Figure S8). Differentiation potential was semi-quantitatively measured in terms of neurite length (**Figure 5B**). All scaffolds supported neurite differentiation as demonstrated by neurite sprouting; while some differences were observed among the different scaffold groups, only the SF-3PD scaffold showed significantly ($p<0.05$) greater average neurite extension compared to unmodified silk. Taking together the biological and physico-chemical results, DMSO-treated PEDOT–PSS functionalized scaffolds tend to outperform their PEDOT–PSS counterparts. Among all scaffolds tested, the SF-3PD group seems to be the best model to take for further assessment.

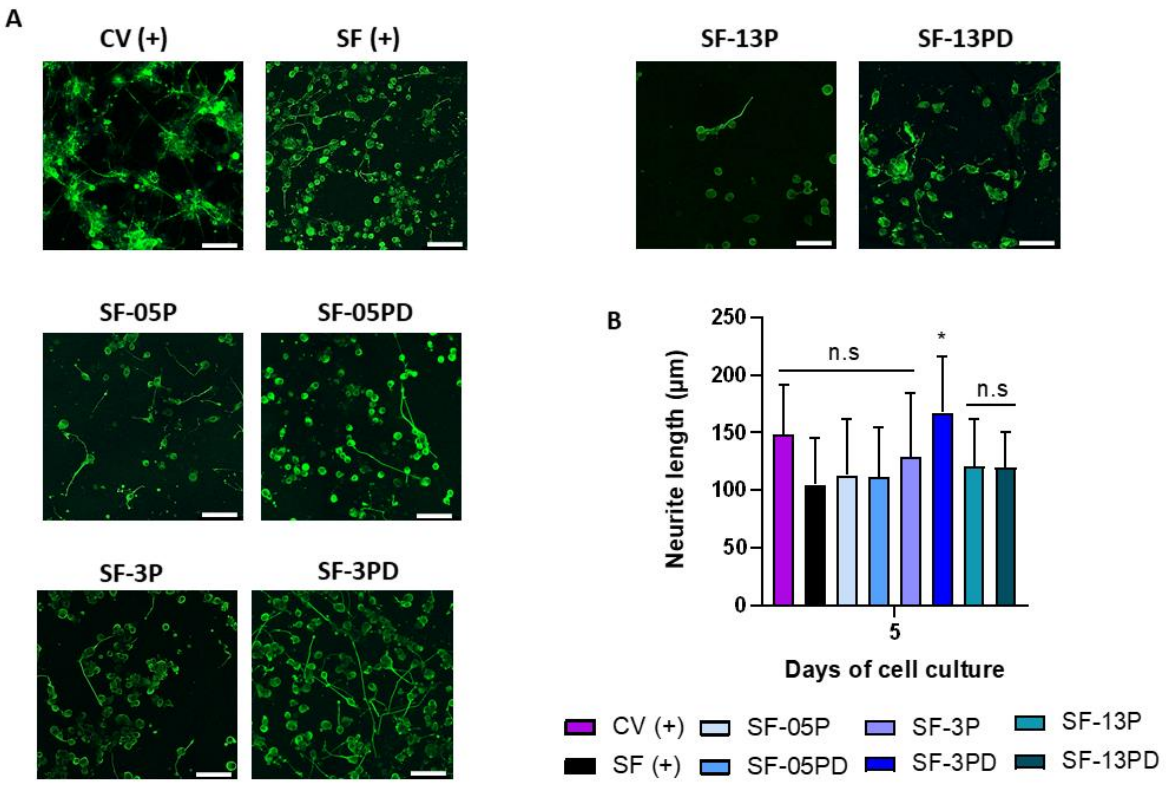

Figure 5 (**A**) Representative confocal micrographs showing differentiated cells on PEDOT–PSS and DMSO-treated PEDOT–PSS functionalized scaffolds (low, medium, and high coating concentration), immunolabeled with ß-tubulin III (green) as a marker of neuronal differentiation and cell nuclei counterstained with DAPI (blue); scale bar at 100 µm. (**B**) Semi-quantitative analysis of the average neurite length on each scaffold (n=2 per type). Differences

between the experimental groups (with respect to silk fibroin) were analyzed by one-way ANOVA with Tukey's post hoc test; n.s non-significant; *$p<0.05$.

The increased cellular responses observed after functionalization may be explained by the presence of PEDOT. Conjugated polymers can interact with and release ions into solution.[10] This in turn may affect ion flux and extracellular membrane potential fluctuations, endowing the scaffold with enhanced biological activity mediated by cell-surface interactions.[65] Furthermore, the inherent electrical conductivity of the substrates and greater protein adsorption observed at increased coating concentration may have played key roles in modulating the cellular response. Previous studies have reported better neuronal PC12 and neuronal stem cell adhesion and proliferation on freeze-dried chitosan/gelatin scaffolds after PEDOT incorporation, along with enhanced differentiation.[9,10] In a subsequent study, cell adhesion efficiency of PC12 neurons and gene expression levels linked to synapse growth were also improved at increased hyaluronic acid-PEDOT content on similarly developed chitosan/gelatin scaffolds.[66] As previously reviewed,[1] some authors have attributed these improvements to the electrostatic interactions between the electroconductive moieties and the negatively charged cell membrane,[67] or to changes in the local electrostatic charge of the scaffold.[56] While the incorporation of an electroconductive enhancer during scaffold synthesis may contribute to increased surface roughness (known to affect protein adsorption and eventual changes in the cellular response such as cell adhesion), differences here were no significant among the different functionalized samples. Therefore, changes in the biological response of the scaffolds may be attributed to the synergic contribution of the endogenous electrical regimen conferred by the presence of PEDOT–PSS and further enhanced by DMSO-treated PEDOT–PSS, enhanced protein adsorption of the substrates, and the more negatively charged (e.g. PEDOT–PSS) or less negatively charged surface (e.g. DMSO-treated PEDOT–PSS) at

the cell-material interface. Indeed, the cell membrane is negatively charged and a possible explanation for the decrease in proliferation observed on the PEDOT–PSS counterparts, as opposed to functionalization with DMSO-treated PEDOT–PSS, is the presence of more anionic PSS chains,[8] as confirmed by HAXPES (**Figure S3**). The lower cellular proliferation observed for the high coating concentration may have been due to reduced inter-fiber porosity (**Figure 1A**), which could have affected initial cell attachment. The presence of DMSO, even in very low concentrations, is known to inhibit neuronal cell activity.[68–70] The fact that the cellular response was not impaired on the DMSO-treated PEDOT–PSS functionalized scaffolds, but rather enhanced over their PEDOT–PSS counterparts, confirms that it is unlikely that there is any presence of DMSO remaining and leaking out into the culture after the preparation steps for cell culture. The cellular response of these scaffolds could be further controlled by grafting multiple combinations of different extracellular matrix (ECM) components such as laminin or peptide sequences known to direct neuronal cell behavior (e.g. IKVAV or GYIGSR).[71] However, grafting such biomolecules on top may impair the endogenous electroconductive stimuli from PEDOT–PSS. One way around is to incorporate into the system inherent electrically conductive biomolecules, such as reflectin[72,73] or melanin,[74,75] with demonstrated efficacy in tissue engineering strategies such as nerve repair.[72,75,76]

Nevertheless, how intracellular cell signaling pathways are specifically modulated to control neuronal cell activity remains to be explored. Integrins and other proteins of the native ECM may redistribute and cluster in response to the conductive polymer, initiating signaling transduction cascades that alter cell behavior.[77] On the other hand, intracellular ion levels such as Ca^{2+} seem to play an important role in regulating neuronal cell behavior.[78–80] In that respect, it has been postulated that conductive substrates may increase intracellular ion levels in neuronal cells.[9,81] Therefore, the contribution of a highly conductive substrate may have

activated specific voltage-ion gated channels of the neuronal cells, leading to the differing cell responses observed. Whether it is conductivity or a cascade of secondary effects, or more likely a synergy of them all, the study presented here represents an important step forward in the benefits of using conductive substrates for regenerating electrically sensitive tissues, and increases our knowledge about the biological response of electrically excitable cells on PEDOT–PSS assembled silk interfaces. The conductivity of native tissue has been reported $\geq 10^{-4}$ S cm^{-1},[82] and therefore the SF-3PD scaffold could be a suitable candidate to be further explored for nerve tissue engineering applications.

4. CONCLUSIONS

Electroconductive fibrous scaffolds were produced by electrospinning, synthesized from naturally occurring silk fibroin protein and functionalized with PEDOT–PSS or DMSO-treated PEDOT–PSS. These functionalized assembled silk-based scaffolds provided an electroconductive environment with enhanced morphological and electrical properties, readily tunable by varying the concentration of PEDOT–PSS and further boosted by DMSO treatment. No significant differences in surface roughness were observed among the different counterparts, but protein adsorption capacity substantially increased in a concentrated-dependent way. The ability of these electroconductive silk scaffolds to modulate growth and differentiation of NG108-15 cells was evaluated *in vitro*. Metabolic activity was enhanced at increased coating concentration compared to unmodified silk, but no differences were observed between DMSO-treated PEDOT–PSS and PEDOT–PSS counterparts. DMSO-treated PEDOT–PSS functionalization led to enhanced cellular proliferation compared to PEDOT–PSS. Cells remained viable in all scaffolds tested, and neurite sprouting was supported during the differentiation phase. Specifically, the SF-3PD scaffold (i.e. DMSO-treated PEDOT–PSS at 3 mg mL^{-1}) showed the best biological outcome among the different concentrations tested

in terms of metabolic activity, cellular proliferation and neuronal differentiation. Overall, these electroconductive scaffolds show promise to potentially be used as platforms for peripheral nerve regeneration, and further investigation should be warranted. The electrical conductivity of these scaffolds in its relation to external electrical stimulation (i.e. direct, capacitive or inductive electrical stimulation) could be explored in the future to further promote neuronal differentiation and neurite outgrowth, along with an electrophysiological study of voltage-gated calcium channels – as well as bioelectronic interfaces for read-outs and sensing.

ASSOCIATED CONTENT

Supporting Information: XPS and HAXPES data, particle size and zeta potential, FTIR-ATR of PEDOT–PSS and DMSO-treated PEDOT–PSS, profilometry micrographs, cellular viability, raw metabolic activity and cellular proliferation, zoomed-in confocal micrographs of neuronal differentiation, estimated PEDOT–PSS mass uptake, concentration and conductivity.

AUTHOR INFORMATION

Corresponding author: *jonny.blaker@manchester.ac.uk

Author Contributions: Conceptualization, X.L, J.G.E and J.J.B.; methodology, A.M and B.F.S; characterization and analysis, A.M and B.F.S; writing—original draft preparation, A.M; writing—review and editing, all authors; supervision, J.G.H, X.L, J.E.G and J.J.B; funding acquisition, X.L, J.E.G and J.J.B.

CONFLICTS OF INTEREST

The authors declare no conflict of interests.

ACKNOWLEDGMENTS

AM acknowledges financial support from The University of Manchester EPSRC DTP (grant no. EP/N509565/1, 1786315) in the United Kingdom, and the Agency for Science Technology and Research (A*STAR) in Singapore via the A*STAR Research Attachment Programme

(ARAP). The authors also thank the Henry Royce Institute for Advanced Materials (grant no. EP/R00661X/1, EP/S019367/1, EP/P025021/1 and EP/P025498/1) for support and equipment use. We would also like to thank Siew Yee Wong at IMRE (A*STAR) for technical support in acquiring FTIR-ATR data.

REFERENCES

(1) Burnstine-Townley, A.; Eshel, Y.; Amdursky, N. Conductive Scaffolds for Cardiac and Neuronal Tissue Engineering: Governing Factors and Mechanisms. *Adv. Funct. Mater.* **2020**, *30* (18), 1901369. https://doi.org/10.1002/adfm.201901369.

(2) Mehrali, M.; Thakur, A.; Pennisi, C. P.; Talebian, S.; Arpanaei, A.; Nikkhah, M.; Dolatshahi-Pirouz, A. Nanoreinforced Hydrogels for Tissue Engineering: Biomaterials That Are Compatible with Load-Bearing and Electroactive Tissues. *Adv. Mater.* **2017**, *29* (8), 1603612. https://doi.org/10.1002/adma.201603612.

(3) Tandon, B.; Magaz, A.; Balint, R.; Blaker, J. J.; Cartmell, S. H. Electroactive Biomaterials: Vehicles for Controlled Delivery of Therapeutic Agents for Drug Delivery and Tissue Regeneration. *Adv. Drug Delivery Rev.* **2018**, *129*, 148–168. https://doi.org/10.1016/j.addr.2017.12.012.

(4) Balint, R.; Cassidy, N. J.; Cartmell, S. H. Conductive Polymers: Towards a Smart Biomaterial for Tissue Engineering. *Acta Biomater.* **2014**, *10* (6), 2341–2353. https://doi.org/10.1016/j.actbio.2014.02.015.

(5) Guimard, N. K.; Gomez, N.; Schmidt, C. E. Conducting Polymers in Biomedical Engineering. *Prog. Polym. Sci.* **2007**, *32* (8), 876–921. https://doi.org/10.1016/j.progpolymsci.2007.05.012.

(6) Tseghai, G. B.; Mengistie, D. A.; Malengier, B.; Fante, K. A.; Van Langenhove, L. PEDOT:PSS-Based Conductive Textiles and Their Applications. *Sensors* **2020**, *20* (7), 1881. https://doi.org/10.3390/s20071881.

(7) Thaning, E. M.; Asplund, M. L. M.; Nyberg, T. A.; Inganäs, O. W.; Holst, H. von. Stability of Poly(3,4-Ethylene Dioxythiophene) Materials Intended for Implants. *J. Biomed. Mater. Res., Part B* **2010**, *93B* (2), 407–415. https://doi.org/10.1002/jbm.b.31597.

(8) Spencer, A. R.; Primbetova, A.; Koppes, A. N.; Koppes, R. A.; Fenniri, H.; Annabi, N. Electroconductive Gelatin Methacryloyl-PEDOT:PSS Composite Hydrogels: Design, Synthesis, and Properties. *ACS Biomater. Sci. Eng.* **2018**, *4* (5), 1558–1567. https://doi.org/10.1021/acsbiomaterials.8b00135.

(9) Wang, S.; Guan, S.; Li, W.; Ge, D.; Xu, J.; Sun, C.; Liu, T.; Ma, X. 3D Culture of Neural Stem Cells within Conductive PEDOT Layer-Assembled Chitosan/Gelatin Scaffolds for Neural Tissue Engineering. *Mater. Sci. Eng. C* **2018**, *93*, 890–901. https://doi.org/10.1016/j.msec.2018.08.054.

(10) Wang, S.; Sun, C.; Guan, S.; Li, W.; Xu, J.; Ge, D.; Zhuang, M.; Liu, T.; Ma, X. Chitosan/Gelatin Porous Scaffolds Assembled with Conductive Poly(3,4-Ethylenedioxythiophene) Nanoparticles for Neural Tissue Engineering. *J. Mater. Chem. B* **2017**, *5* (24), 4774–4788. https://doi.org/10.1039/C7TB00608J.

(11) Roshanbinfar, K.; Vogt, L.; Greber, B.; Diecke, S.; Boccaccini, A. R.; Scheibel, T.; Engel, F. B. Electroconductive Biohybrid Hydrogel for Enhanced Maturation and

Beating Properties of Engineered Cardiac Tissues. *Adv. Funct. Mater.* **2018**, *28* (42), 1803951. https://doi.org/10.1002/adfm.201803951.

(12) Solazzo, M.; O'Brien, F. J.; Nicolosi, V.; Monaghan, M. G. The Rationale and Emergence of Electroconductive Biomaterial Scaffolds in Cardiac Tissue Engineering. *APL Bioeng.* **2019**, *3* (4), 041501. https://doi.org/10.1063/1.5116579.

(13) Yildirim, E.; Wu, G.; Yong, X.; Tan, T. L.; Zhu, Q.; Xu, J.; Ouyang, J.; Wang, J.-S.; Yang, S.-W. A Theoretical Mechanistic Study on Electrical Conductivity Enhancement of DMSO Treated PEDOT:PSS. *J. Mater. Chem. C* **2018**, *6* (19), 5122–5131. https://doi.org/10.1039/C8TC00917A.

(14) El Zein, A.; Huppé, C.; Cochrane, C. Development of a Flexible Strain Sensor Based on PEDOT:PSS for Thin Film Structures. *Sensors* **2017**, *17* (6), 1337. https://doi.org/10.3390/s17061337.

(15) Pot, S. A.; Liliensiek, S. J.; Myrna, K. E.; Bentley, E.; Jester, J. V.; Nealey, P. F.; Murphy, C. J. Nanoscale Topography–Induced Modulation of Fundamental Cell Behaviors of Rabbit Corneal Keratocytes, Fibroblasts, and Myofibroblasts. *Invest Ophthalmol Vis Sci* **2010**, *51* (3), 1373–1381. https://doi.org/10.1167/iovs.09-4074.

(16) Ahn, E. H.; Kim, Y.; Kshitiz; An, S. S.; Afzal, J.; Lee, S.; Kwak, M.; Suh, K.-Y.; Kim, D.-H.; Levchenko, A. Spatial Control of Adult Stem Cell Fate Using Nanotopographic Cues. *Biomaterials* **2014**, *35* (8), 2401–2410. https://doi.org/10.1016/j.biomaterials.2013.11.037.

(17) Li, W.-J.; Cooper, J. A. Fibrous Scaffolds for Tissue Engineering. In *Biomaterials for Tissue Engineering Applications*; Springer, Vienna, 2011; pp 47–73. https://doi.org/10.1007/978-3-7091-0385-2_3.

(18) Shamsah, A. H.; Cartmell, S. H.; Richardson, S. M.; Bosworth, L. A. Tissue Engineering the Annulus Fibrosus Using 3D Rings of Electrospun PCL:PLLA Angle-Ply Nanofiber Sheets. *Front Bioeng Biotechnol* **2020**, *7*, 437. https://doi.org/10.3389/fbioe.2019.00437.

(19) Das, S.; Sharma, M.; Saharia, D.; Sarma, K. K.; Sarma, M. G.; Borthakur, B. B.; Bora, U. In Vivo Studies of Silk Based Gold Nano-Composite Conduits for Functional Peripheral Nerve Regeneration. *Biomaterials* **2015**, *62*, 66–75. https://doi.org/10.1016/j.biomaterials.2015.04.047.

(20) Alessandrino, A.; Fregnan, F.; Biagiotti, M.; Muratori, L.; Bassani, G. A.; Ronchi, G.; Vincoli, V.; Pierimarchi, P.; Geuna, S.; Freddi, G. SilkBridge^{TM}: A Novel Biomimetic and Biocompatible Silk-Based Nerve Conduit. *Biomater. Sci.* **2019**, *7* (10), 4112–4130. https://doi.org/10.1039/C9BM00783K.

(21) Altman, G. H.; Diaz, F.; Jakuba, C.; Calabro, T.; Horan, R. L.; Chen, J.; Lu, H.; Richmond, J.; Kaplan, D. L. Silk-Based Biomaterials. *Biomaterials* **2003**, *24* (3), 401–416. https://doi.org/10.1016/s0142-9612(02)00353-8.

(22) Das, S.; Bora, U.; Borthakur, B. B. 2 - Applications of Silk Biomaterials in Tissue Engineering and Regenerative Medicine. In *Silk Biomaterials for Tissue Engineering and Regenerative Medicine*; Kundu, S. C., Ed.; Woodhead Publishing, 2014; pp 41–77. https://doi.org/10.1533/9780857097064.1.41.

(23) Magaz, A.; Faroni, A.; Gough, J. E.; Reid, A. J.; Li, X.; Blaker, J. J. Bioactive Silk-Based Nerve Guidance Conduits for Augmenting Peripheral Nerve Repair. *Adv. Healthc. Mater.* **2018**, *7* (23), 1800308. https://doi.org/10.1002/adhm.201800308.

(24) Xia, Y.; Lu, Y. Fabrication and Properties of Conductive Conjugated Polymers/Silk Fibroin Composite Fibers. *Compos. Sci. Technol.* **2008**, *68* (6), 1471–1479. https://doi.org/10.1016/j.compscitech.2007.10.044.

(25) Müller, C.; Jansson, R.; Elfwing, A.; Askarieh, G.; Karlsson, R.; Hamedi, M.; Rising, A.; Johansson, J.; Inganäs, O.; Hedhammar, M. Functionalisation of Recombinant Spider Silk with Conjugated Polyelectrolytes. *J. Mater. Chem.* **2011**, *21* (9), 2909–2915. https://doi.org/10.1039/C0JM03270K.

(26) Tsukada, S.; Nakashima, H.; Torimitsu, K. Conductive Polymer Combined Silk Fiber Bundle for Bioelectrical Signal Recording. *PLoS ONE* **2012**, *7* (4), 33689. https://doi.org/10.1371/journal.pone.0033689.

(27) Müller, C.; Hamedi, M.; Karlsson, R.; Jansson, R.; Marcilla, R.; Hedhammar, M.; Inganäs, O. Woven Electrochemical Transistors on Silk Fibers. *Adv. Mater.* **2011**, *23* (7), 898–901. https://doi.org/10.1002/adma.201003601.

(28) Ryan, J. D.; Mengistie, D. A.; Gabrielsson, R.; Lund, A.; Müller, C. Machine-Washable PEDOT:PSS Dyed Silk Yarns for Electronic Textiles. *ACS Appl. Mater. Interfaces* **2017**, *9* (10), 9045–9050. https://doi.org/10.1021/acsami.7b00530.

(29) Jiang, Y.; Xu, M.; Yadavalli, V. K. Silk Fibroin-Sheathed Conducting Polymer Wires as Organic Connectors for Biosensors. *Biosensors* **2019**, *9* (3), 103. https://doi.org/10.3390/bios9030103.

(30) Severt, S. Y.; Ostrovsky-Snider, N. A.; Leger, J. M.; Murphy, A. R. Versatile Method for Producing 2D and 3D Conductive Biomaterial Composites Using Sequential Chemical and Electrochemical Polymerization. *ACS Appl. Mater. Interfaces* **2015**, *7* (45), 25281–25288. https://doi.org/10.1021/acsami.5b07332.

(31) Teshima, T.; Nakashima, H.; Kasai, N.; Sasaki, S.; Tanaka, A.; Tsukada, S.; Sumitomo, K. Mobile Silk Fibroin Electrode for Manipulation and Electrical Stimulation of Adherent Cells. *Adv. Funct. Mater.* **2016**, *26* (45), 8185–8193. https://doi.org/10.1002/adfm.201603302.

(32) Pal, R. K.; Farghaly, A. A.; Collinson, M. M.; Kundu, S. C.; Yadavalli, V. K. Photolithographic Micropatterning of Conducting Polymers on Flexible Silk Matrices. *Adv. Mater.* **2016**, *28* (7), 1406–1412. https://doi.org/10.1002/adma.201504736.

(33) Dodel, M.; Hemmati Nejad, N.; Bahrami, S. H.; Soleimani, M.; Mohammadi Amirabad, L.; Hanaee-Ahvaz, H.; Atashi, A. Electrical Stimulation of Somatic Human Stem Cells Mediated by Composite Containing Conductive Nanofibers for Ligament Regeneration. *Biologicals* **2017**, *46*, 99–107. https://doi.org/10.1016/j.biologicals.2017.01.007.

(34) Magaz, A.; Roberts, A. D.; Faraji, S.; Nascimento, T. R. L.; Medeiros, E. S.; Zhang, W.; Greenhalgh, R. D.; Mautner, A.; Li, X.; Blaker, J. J. Porous, Aligned, and Biomimetic Fibers of Regenerated Silk Fibroin Produced by Solution Blow Spinning. *Biomacromolecules* **2018**, *19* (12), 4542–4553. https://doi.org/10.1021/acs.biomac.8b01233.

(35) Matsumoto, A.; Chen, J.; Collette, A. L.; Kim, U.-J.; Altman, G. H.; Cebe, P.; Kaplan, D. L. Mechanisms of Silk Fibroin Sol−gel Transitions. *J. Phys. Chem. B* **2006**, *110* (43), 21630–21638. https://doi.org/10.1021/jp056350v.

(36) Shen, G.; Hu, X.; Guan, G.; Wang, L. Surface Modification and Characterisation of Silk Fibroin Fabric Produced by the Layer-by-Layer Self-Assembly of Multilayer Alginate/Regenerated Silk Fibroin. *PLoS ONE* **2015**, *10* (4), 0124811. https://doi.org/10.1371/journal.pone.0124811.

(37) Dickhaus, B. N.; Priefer, R. Determination of Polyelectrolyte PKa Values Using Surface-to-Air Tension Measurements. *Colloids and Surfaces A: Physicochemical and Engineering Aspects* **2016**, *488*, 15–19. https://doi.org/10.1016/j.colsurfa.2015.10.015.

(38) Regoutz, A.; Mascheck, M.; Wiell, T.; Eriksson, S. K.; Liljenberg, C.; Tetzner, K.; Williamson, B. A. D.; Scanlon, D. O.; Palmgren, P. A Novel Laboratory-Based Hard

X-Ray Photoelectron Spectroscopy System. *Review of Scientific Instruments* **2018**, *89* (7), 073105. https://doi.org/10.1063/1.5039829.

(39) Spencer, B. F.; Maniyarasu, S.; Reed, B.; Cant, D. J. H.; Ahumada-Lazo, R.; Thomas, A. G.; Muryn, C. A.; Maschek, M.; Eriksson, S. K.; Wiell, T.; Lee, T. L.; Tougaard, S. T.; Shard, A. G.; Flavell, W. R. Dataset: Hard X-Rays and Inelastic Background Modelling Extend Photoelectron Spectroscopy below the Surface for the Detection of Buried Layers. *Applied Surface Science* **2020**, *[in peer review]*. https://doi.org/10.17632/8d62nnf57b.1.

(40) Alhummiany, H.; Rafique, S.; Sulaiman, K. XPS Analysis of the Improved Operational Stability of Organic Solar Cells Using a V2O5 and PEDOT:PSS Composite Layer: Effect of Varied Atmospheric Conditions. *J. Phys. Chem. C* **2017**, *121* (14), 7649–7658. https://doi.org/10.1021/acs.jpcc.6b13016.

(41) Kai, D.; Prabhakaran, M. P.; Jin, G.; Ramakrishna, S. Biocompatibility Evaluation of Electrically Conductive Nanofibrous Scaffolds for Cardiac Tissue Engineering. *J. Mater. Chem. B* **2013**, *1* (17), 2305–2314. https://doi.org/10.1039/C3TB00151B.

(42) Zhao, G.; Qing, H.; Huang, G.; Genin, G. M.; Lu, T. J.; Luo, Z.; Xu, F.; Zhang, X. Reduced Graphene Oxide Functionalized Nanofibrous Silk Fibroin Matrices for Engineering Excitable Tissues. *NPG Asia Mater.* **2018**, *10* (10), 982. https://doi.org/10.1038/s41427-018-0092-8.

(43) Whitemarsh, R. C. M.; Pier, C. L.; Tepp, W. H.; Pellett, S.; Johnson, E. A. Model for Studying Clostridium Botulinum Neurotoxin Using Differentiated Motor Neuron-like NG108-15 Cells. *Biochem Biophys Res Commun* **2012**, *427* (2), 426–430. https://doi.org/10.1016/j.bbrc.2012.09.082.

(44) Serth, J.; Kuczyk, M. A.; Paeslack, U.; Lichtinghagen, R.; Jonas, U. Quantitation of DNA Extracted after Micropreparation of Cells from Frozen and Formalin-Fixed Tissue Sections. *Am. J. Pathol.* **2000**, *156* (4), 1189–1196. https://doi.org/10.1016/S0002-9440(10)64989-9.

(45) Ouyang, J.; Xu, Q.; Chu, C.-W.; Yang, Y.; Li, G.; Shinar, J. On the Mechanism of Conductivity Enhancement in Poly(3,4-Ethylenedioxythiophene):Poly(Styrene Sulfonate) Film through Solvent Treatment. *Polym. J.* **2004**, *45* (25), 8443–8450. https://doi.org/10.1016/j.polymer.2004.10.001.

(46) Gonzalez-Perez, F.; Udina, E.; Navarro, X. Chapter 10- Extracellular Matrix Components in Peripheral Nerve Regeneration. In *International Review of Neurobiology*; Geuna, S., Perroteau, I., Tos, P., Battiston, B., Eds.; Tissue Engineering of the Peripheral Nerve: Stem Cells and Regeneration Promoting Factors; Academic Press, 2013; Vol. 108, pp 257–275. https://doi.org/10.1016/B978-0-12-410499-0.00010-1.

(47) Ghobeira, R.; Asadian, M.; Vercruysse, C.; Declercq, H.; De Geyter, N.; Morent, R. Wide-Ranging Diameter Scale of Random and Highly Aligned PCL Fibers Electrospun Using Controlled Working Parameters. *Polymer* **2018**, *157*, 19–31. https://doi.org/10.1016/j.polymer.2018.10.022.

(48) Song, Y.; Wang, Y.; Xu, L.; Wang, M. Fabrication and Characterization of Electrospun Aligned Porous PAN/Graphene Composite Nanofibers. *Nanomaterials (Basel)* **2019**, *9* (12). https://doi.org/10.3390/nano9121782.

(49) Lingstedt, L. V.; Ghittorelli, M.; Lu, H.; Koutsouras, D. A.; Marszalek, T.; Torricelli, F.; Crăciun, N. I.; Gkoupidenis, P.; Blom, P. W. M. Effect of DMSO Solvent Treatments on the Performance of PEDOT:PSS Based Organic Electrochemical Transistors. *Advanced Electronic Materials* **2019**, *5* (3), 1800804. https://doi.org/10.1002/aelm.201800804.

(50) Li, Q.; Yang, J.; Chen, S.; Zou, J.; Xie, W.; Zeng, X. Highly Conductive PEDOT:PSS Transparent Hole Transporting Layer with Solvent Treatment for High Performance Silicon/Organic Hybrid Solar Cells. *Nanoscale Research Letters* **2017**, *12* (1), 506. https://doi.org/10.1186/s11671-017-2276-5.

(51) Ghasemi-Mobarakeh, L.; Prabhakaran, M. P.; Tian, L.; Shamirzaei-Jeshvaghani, E.; Dehghani, L.; Ramakrishna, S. Structural Properties of Scaffolds: Crucial Parameters towards Stem Cells Differentiation. *World J Stem Cells* **2015**, *7* (4), 728–744. https://doi.org/10.4252/wjsc.v7.i4.728.

(52) Rechendorff, K.; Hovgaard, M. B.; Foss, M.; Zhdanov, V. P.; Besenbacher, F. Enhancement of Protein Adsorption Induced by Surface Roughness. *Langmuir* **2006**, *22* (26), 10885–10888. https://doi.org/10.1021/la0621923.

(53) Biazar, E.; Heidari, M.; Asefnezhad, A.; Montazeri, N. The Relationship between Cellular Adhesion and Surface Roughness in Polystyrene Modified by Microwave Plasma Radiation. *Int J Nanomedicine* **2011**, *6*, 631–639. https://doi.org/10.2147/IJN.S17218.

(54) McUmber, A. C.; Randolph, T. W.; Schwartz, D. K. Electrostatic Interactions Influence Protein Adsorption (but Not Desorption) at the Silica–Aqueous Interface. *J. Phys. Chem. Lett.* **2015**, *6* (13), 2583–2587. https://doi.org/10.1021/acs.jpclett.5b00933.

(55) van der Veen, M.; Norde, W.; Stuart, M. C. Electrostatic Interactions in Protein Adsorption Probed by Comparing Lysozyme and Succinylated Lysozyme. *Colloids Surf B Biointerfaces* **2004**, *35* (1), 33–40. https://doi.org/10.1016/j.colsurfb.2004.02.005.

(56) Kotwal, A.; Schmidt, C. E. Electrical Stimulation Alters Protein Adsorption and Nerve Cell Interactions with Electrically Conducting Biomaterials. *Biomaterials* **2001**, *22* (10), 1055–1064. https://doi.org/10.1016/S0142-9612(00)00344-6.

(57) Medda, L.; Monduzzi, M.; Salis, A. The Molecular Motion of Bovine Serum Albumin under Physiological Conditions Is Ion Specific. *Chem Commun* **2015**, *51* (30), 6663–6666. https://doi.org/10.1039/C5CC01538C.

(58) Tulachan, B.; Meena, S. K.; Rai, R. K.; Mallick, C.; Kusurkar, T. S.; Teotia, A. K.; Sethy, N. K.; Bhargava, K.; Bhattacharya, S.; Kumar, A.; Sharma, R. K.; Sinha, N.; Singh, S. K.; Das, M. Electricity from the Silk Cocoon Membrane. *Sci Rep* **2014**, *4*, 5434.

(59) Ouyang, J. "Secondary Doping" Methods to Significantly Enhance the Conductivity of PEDOT:PSS for Its Application as Transparent Electrode of Optoelectronic Devices. *Displays* **2013**, *34* (5), 423–436. https://doi.org/10.1016/j.displa.2013.08.007.

(60) Pathak, C. S.; Singh, J. P.; Singh, R. Effect of Dimethyl Sulfoxide on the Electrical Properties of PEDOT:PSS/n-Si Heterojunction Diodes. *Curr. Appl. Phys.* **2015**, *15* (4), 528–534. https://doi.org/10.1016/j.cap.2015.01.020.

(61) Martins, A. M.; Eng, G.; Caridade, S. G.; Mano, J. F.; Reis, R. L.; Vunjak-Novakovic, G. Electrically Conductive Chitosan/Carbon Scaffolds for Cardiac Tissue Engineering. *Biomacromolecules* **2014**, *15* (2), 635–643. https://doi.org/10.1021/bm401679q.

(62) Kwak, H. W.; Eom, J.; Cho, S. Y.; Lee, M. E.; Jin, H.-J. High-Toughness Natural Polymer Nonwoven Preforms Inspired by Silkworm Cocoon Structure. *Int. J. Biol. Macromol.* **2019**, *127*, 146–152. https://doi.org/10.1016/j.ijbiomac.2019.01.005.

(63) Zhu, Z.; Song, H.; Xu, J.; Liu, C.; Jiang, Q.; Shi, H. Significant Conductivity Enhancement of PEDOT:PSS Films Treated with Lithium Salt Solutions. *J Mater Sci: Mater Electron* **2015**, *26* (1), 429–434. https://doi.org/10.1007/s10854-014-2417-x.

(64) Döbbelin, M.; Marcilla, R.; Tollan, C.; A. Pomposo, J.; Sarasua, J.-R.; Mecerreyes, D. A New Approach to Hydrophobic and Water-Resistant Poly(3,4-Ethylenedioxythiophene):Poly(Styrenesulfonate) Films Using Ionic Liquids. *Journal of Materials Chemistry* **2008**, *18* (44), 5354–5358. https://doi.org/10.1039/B808723G.

(65) Blau, A. Cell Adhesion Promotion Strategies for Signal Transduction Enhancement in Microelectrode Array in Vitro Electrophysiology: An Introductory Overview and Critical Discussion. *Curr. Opin. Colloid Interface Sci.* **2013**, *18* (5), 481–492. https://doi.org/10.1016/j.cocis.2013.07.005.

(66) Wang, S.; Guan, S.; Zhu, Z.; Li, W.; Liu, T.; Ma, X. Hyaluronic Acid Doped-Poly(3,4-Ethylenedioxythiophene)/Chitosan/Gelatin (PEDOT-HA/Cs/Gel) Porous Conductive Scaffold for Nerve Regeneration. *Mater Sci Eng C* **2017**, *71*, 308–316. https://doi.org/10.1016/j.msec.2016.10.029.

(67) Mihardja, S. S.; Sievers, R. E.; Lee, R. J. The Effect of Polypyrrole on Arteriogenesis in an Acute Rat Infarct Model. *Biomaterials* **2008**, *29* (31), 4205–4210. https://doi.org/10.1016/j.biomaterials.2008.07.021.

(68) Zhang, C.; Deng, Y.; Dai, H.; Zhou, W.; Tian, J.; Bing, G.; Zhao, L. Effects of Dimethyl Sulfoxide on the Morphology and Viability of Primary Cultured Neurons and Astrocytes. *Brain Res. Bull.* **2017**, *128*, 34–39. https://doi.org/10.1016/j.brainresbull.2016.11.004.

(69) Radio, N. M.; Breier, J. M.; Shafer, T. J.; Mundy, W. R. Assessment of Chemical Effects on Neurite Outgrowth in PC12 Cells Using High Content Screening. *Toxicol Sci* **2008**, *105* (1), 106–118. https://doi.org/10.1093/toxsci/kfn114.

(70) O'Sullivan, A.; Lange, S.; Rotheneichner, P.; Bieler, L.; Aigner, L.; Rivera, F. J.; Couillard-Despres, S. Dimethylsulfoxide Inhibits Oligodendrocyte Fate Choice of Adult Neural Stem and Progenitor Cells. *Front. Neurosci.* **2019**, *13*. https://doi.org/10.3389/fnins.2019.01242.

(71) Manchineella, S.; Thrivikraman, G.; Basu, B.; Govindaraju, T. Surface-Functionalized Silk Fibroin Films as a Platform to Guide Neuron-like Differentiation of Human Mesenchymal Stem Cells. *ACS Appl. Mater. Interfaces* **2016**, *8* (35), 22849–22859. https://doi.org/10.1021/acsami.6b06403.

(72) Phan, L.; Kautz, R.; Arulmoli, J.; Kim, I. H.; Le, D. T. T.; Shenk, M. A.; Pathak, M. M.; Flanagan, L. A.; Tombola, F.; Gorodetsky, A. A. Reflectin as a Material for Neural Stem Cell Growth. *ACS Appl Mater Interfaces* **2016**, *8* (1), 278–284. https://doi.org/10.1021/acsami.5b08717.

(73) D. Ordinario, D.; Phan, L.; Iv, W. G. W.; Dyke, Y. V.; M. Leung, E.; Nguyen, M.; G. Smith, A.; Kerr, J.; Naeim, M.; Kymissis, I.; A. Gorodetsky, A. Production and Electrical Characterization of the Reflectin A2 Isoform from Doryteuthis (Loligo) Pealeii. *RSC Adv* **2016**, *6* (62), 57103–57107. https://doi.org/10.1039/C6RA05405F.

(74) Manchineella, S.; Thrivikraman, G.; Khanum, K. K.; Ramamurthy, P. C.; Basu, B.; Govindaraju, T. Pigmented Silk Nanofibrous Composite for Skeletal Muscle Tissue Engineering. *Adv. Healthcare Mater.* **2016**, *5* (10), 1222–1232. https://doi.org/10.1002/adhm.201501066.

(75) Nune, M.; Manchineella, S.; T., G.; K.s., N. Melanin Incorporated Electroactive and Antioxidant Silk Fibroin Nanofibrous Scaffolds for Nerve Tissue Engineering. *Materials Science and Engineering: C* **2019**, *94*, 17–25. https://doi.org/10.1016/j.msec.2018.09.014.

(76) Gevorkyan, Olga. V.; Meliksetyan, I. B.; Petrosyan, T. R.; Hovsepyan, A. S. Bacterial Melanin Promotes Recovery after Sciatic Nerve Injury in Rats. *Neural Regen Res* **2015**, *10* (1), 124–127. https://doi.org/10.4103/1673-5374.150719.

(77) Zhang, J.; Li, M.; Kang, E.-T.; Neoh, K. G. Electrical Stimulation of Adipose-Derived Mesenchymal Stem Cells in Conductive Scaffolds and the Roles of Voltage-Gated Ion Channels. *Acta Biomater* **2016**, *32*, 46–56. https://doi.org/10.1016/j.actbio.2015.12.024.

(78) Sheng, L.; Leshchyns'ka, I.; Sytnyk, V. Neural Cell Adhesion Molecule 2 Promotes the Formation of Filopodia and Neurite Branching by Inducing Submembrane Increases in Ca2+ Levels. *J. Neurosci.* **2015**, *35* (4), 1739–1752. https://doi.org/10.1523/JNEUROSCI.1714-14.2015.

(79) Zamburlin, P.; Ruffinatti, F. A.; Gilardino, A.; Farcito, S.; Parrini, M.; Lovisolo, D. Calcium Signals and FGF-2 Induced Neurite Growth in Cultured Parasympathetic Neurons: Spatial Localization and Mechanisms of Activation. *Pflugers Arch - Eur J Physiol* **2013**, *465* (9), 1355–1370. https://doi.org/10.1007/s00424-013-1257-5.

(80) Zatkova, M.; Reichova, A.; Bacova, Z.; Strbak, V.; Kiss, A.; Bakos, J. Neurite Outgrowth Stimulated by Oxytocin Is Modulated by Inhibition of the Calcium Voltage-Gated Channels. *Cell Mol Neurobiol* **2018**, *38* (1), 371–378. https://doi.org/10.1007/s10571-017-0503-3.

(81) Guo, R.; Zhang, S.; Xiao, M.; Qian, F.; He, Z.; Li, D.; Zhang, X.; Li, H.; Yang, X.; Wang, M.; Chai, R.; Tang, M. Accelerating Bioelectric Functional Development of Neural Stem Cells by Graphene Coupling: Implications for Neural Interfacing with Conductive Materials. *Biomaterials* **2016**, *106*, 193–204. https://doi.org/10.1016/j.biomaterials.2016.08.019.

(82) Gabriel, C.; Gabriel, S.; Corthout, E. The Dielectric Properties of Biological Tissues: I. Literature Survey. *Phys. Med. Biol.* **1996**, *41* (11), 2231–2249. https://doi.org/10.1088/0031-9155/41/11/001.

GRAPHIC TOC

For Table of Contents Use Only

Modulation of neuronal cell affinity on PEDOT–PSS non-woven silk scaffolds for neural tissue engineering

Adrián Magaz, Ben F. Spencer, John G. Hardy, Xu Li, Julie E. Gough, Jonny J. Blaker